

NEUROSCIENCE

An action potential initiation mechanism in distal axons for the control of dopamine release

Changliang Liu^{1*}, Xintong Cai¹, Andreas Ritzau-Jost², Paul F. Kramer³, Yulong Li⁴, Zayd M. Khaliq³, Stefan Hallermann², Pascal S. Kaeser^{1*}

Information flow in neurons proceeds by integrating inputs in dendrites, generating action potentials near the soma, and releasing neurotransmitters from nerve terminals in the axon. We found that in the striatum, acetylcholine-releasing neurons induce action potential firing in distal dopamine axons. Spontaneous activity of cholinergic neurons produced dopamine release that extended beyond acetylcholine-signaling domains, and traveling action potentials were readily recorded from dopamine axons in response to cholinergic activation. In freely moving mice, dopamine and acetylcholine covaried with movement direction. Local inhibition of nicotinic acetylcholine receptors impaired dopamine dynamics and affected movement. Our findings uncover an endogenous mechanism for action potential initiation independent of somatodendritic integration and establish that this mechanism segregates the control of dopamine signaling between axons and somata.

Neurons receive input through dendrites and send output through axons. Although axonal function is regulated locally, it is thought that distal axons are not equipped with endogenous, physiological mechanisms for action potential induction. Midbrain dopamine neurons innervate the striatum with extensively arborized axons to regulate a wide variety of functions (1–4). Of striatal neurons, 1 to 3% are tonically active interneurons that release acetylcholine (ACh), and their axons intertwine with those of dopamine neurons (5, 6). Dopamine axons express high levels of nicotinic ACh receptors (nAChRs), and synchronous activation of these receptors can drive dopamine release directly (6–12). Hence, distal dopamine axons are under local striatal control and can release dopamine independent of activity ascending from their midbrain somata. However, because the command for neurotransmitter release generally originates from the soma, fundamental questions remain as to how nAChR activation is translated into dopamine release and whether this process represents a bona fide regulation used by the dopamine system.

The striatal cholinergic system broadcasts dopamine release

We expressed GRAB_{DA2m} [abbreviated as GRAB_{DA}, a D2 receptor-based dopamine sensor (13); GRAB, a G protein-coupled receptor (GPCR) activation-based] in midbrain dopamine neurons and monitored fluorescence changes in acute striatal slices (Fig. 1A). Restricting GRAB_{DA} expression to dopamine axons provides a widespread

sensor network in the striatum and facilitates detection because the sensors are present in the immediate vicinity of dopamine release (Fig. 1B). Dopamine release was detected in both dorsal and ventral striatum without any stimulation, and this spontaneous release was sensitive to DHβE, a blocker of β2-containing nAChRs (Fig. 1, A to E; fig. S1A; and movie S1). Release occurred stochastically and exhibited all-or-none properties: Either an event covered a large area, estimated to contain 3 million to 15 million dopamine terminals (14), or no release was detected (Fig. 1C and fig. S1C). Because midbrain dopamine cell bodies are absent in this striatal slice preparation, the detected release is induced without involvement of dopamine neuron somata.

Using a corresponding strategy with GRAB_{ACh30} [abbreviated as GRAB_{ACh}, an M3-receptor-based ACh sensor (15)], we also detected spontaneous ACh release in both dorsal and ventral striatum, which is consistent with previous work on spontaneous ACh neuron activity (16). ACh release was sensitive to the sodium channel blocker tetrodotoxin (TTX) and exhibited an all-or-none pattern like that of dopamine (Fig. 1, F and G; fig. S1, A to C; and movie S2). The frequency of ACh release was approximately threefold higher than that of dopamine release, suggesting that not all ACh triggers dopamine release (Fig. 1, E and G). Although less frequent, areas covered by dopamine release were approximately three times larger compared with those of ACh (Fig. 1H). Adjusting event detection thresholds or enhancing GRAB_{ACh} expression by injecting the respective adeno-associated virus (AAV) directly into the striatum slightly influenced the signals (fig. S1, D to G), but dopamine release continued to be less frequent and broader than ACh release. Increasing slice thickness enhanced dopamine release frequency, but blocking synaptic transmission only marginally influenced dopamine and ACh release (fig. S2).

Cholinergic interneurons exhibit multiple firing activities: They have spontaneous pacemaker activity and respond with pause-rebound firing *in vivo* to a variety of sensory stimuli (17–20). Because spontaneous cholinergic activity drives dopamine release stochastically (Fig. 1, C and D), we speculated that pause-rebound firing might induce time-locked dopamine release. We mimicked ACh pause-rebound activity in striatal slices and found that it induces a robust dopamine transient during rebound firing (fig. S3).

We next evoked dopamine and ACh release using electrical stimulation (Fig. 1, I to S). A large proportion of electrically evoked dopamine release was driven by activation of nAChRs (Fig. 1, I and J) (6, 10, 12, 14). Consistent with the findings from spontaneous release, evoked dopamine release covered an area three to four times larger than that of evoked ACh release, and nAChR blockade strongly reduced its area (Fig. 1, K and O). Similar results were obtained when ACh and dopamine release were measured simultaneously [with GRAB_{ACh} and rGRAB_{DA1h}, abbreviated as rGRAB_{DA}, a red-shifted dopamine sensor (13)], and the release areas were positively correlated with one another (Fig. 1, Q to S).

Dopamine release with nAChR activation depressed more strongly during repetitive stimulation than release evoked without it (Fig. 1 I to L) (12, 14). This is thought to be a result of rapid nAChR desensitization, but our data indicate that it is most likely caused by depression of ACh release after the first stimulus (Fig. 1, M to P). The depression of ACh release was attenuated by blocking nAChRs or D2 receptors, but not AMPA, *N*-methyl-D-aspartate (NMDA), or γ-aminobutyric acid type A (GABA_A) receptors (Fig. 1P and fig. S4, A to D), suggesting that it is due to feedback inhibition mediated by dopamine. Blocking nAChRs or D2 receptors also increased ACh release in response to the first stimulus (Fig. 1, M to O, and fig. S4, E to G), likely because ACh release is tonically inhibited by dopamine (18).

ACh- and action potential-induced dopamine secretion share release mechanisms

We next asked why dopamine release spreads beyond the area of ACh release (Fig. 1, Q to S). We first examined the organization of striatal ACh terminals and dopamine axons using superresolution three-dimensional structured illumination microscopy (3D-SIM). Although synaptophysin-tdTomato-labeled ACh terminals were intermingled with tyrosine hydroxylase (TH)-labeled dopamine axons, no prominent association was detected (8, 27), and their contact frequency was much lower than the density of release sites in dopamine axons (Fig. 2, A and B) (14).

Dopamine axons contain varicosities that are filled with vesicles, but only a small fraction

¹Department of Neurobiology, Harvard Medical School, Boston, MA, USA. ²Carl-Ludwig-Institute of Physiology, Faculty of Medicine, Leipzig University, Leipzig, Germany. ³Cellular Neurophysiology Section, National Institute of Neurological Disorders and Stroke, National Institutes of Health, Bethesda, MD, USA. ⁴State Key Laboratory of Membrane Biology, Peking University School of Life Sciences, Beijing, China.

*Corresponding author. Email: changliang_liu@hms.harvard.edu (C.L.); kaeser@hms.harvard.edu (P.S.K.)

Fig. 1. ACh-induced dopamine secretion expands beyond ACh release.

(A) Schematic of midbrain AAV injection for dopamine axonal expression of GRAB_{DA}, rGRAB_{DA}, or GRAB_{ACh} sensors followed by widefield fluorescence imaging in parasagittal striatal slices.

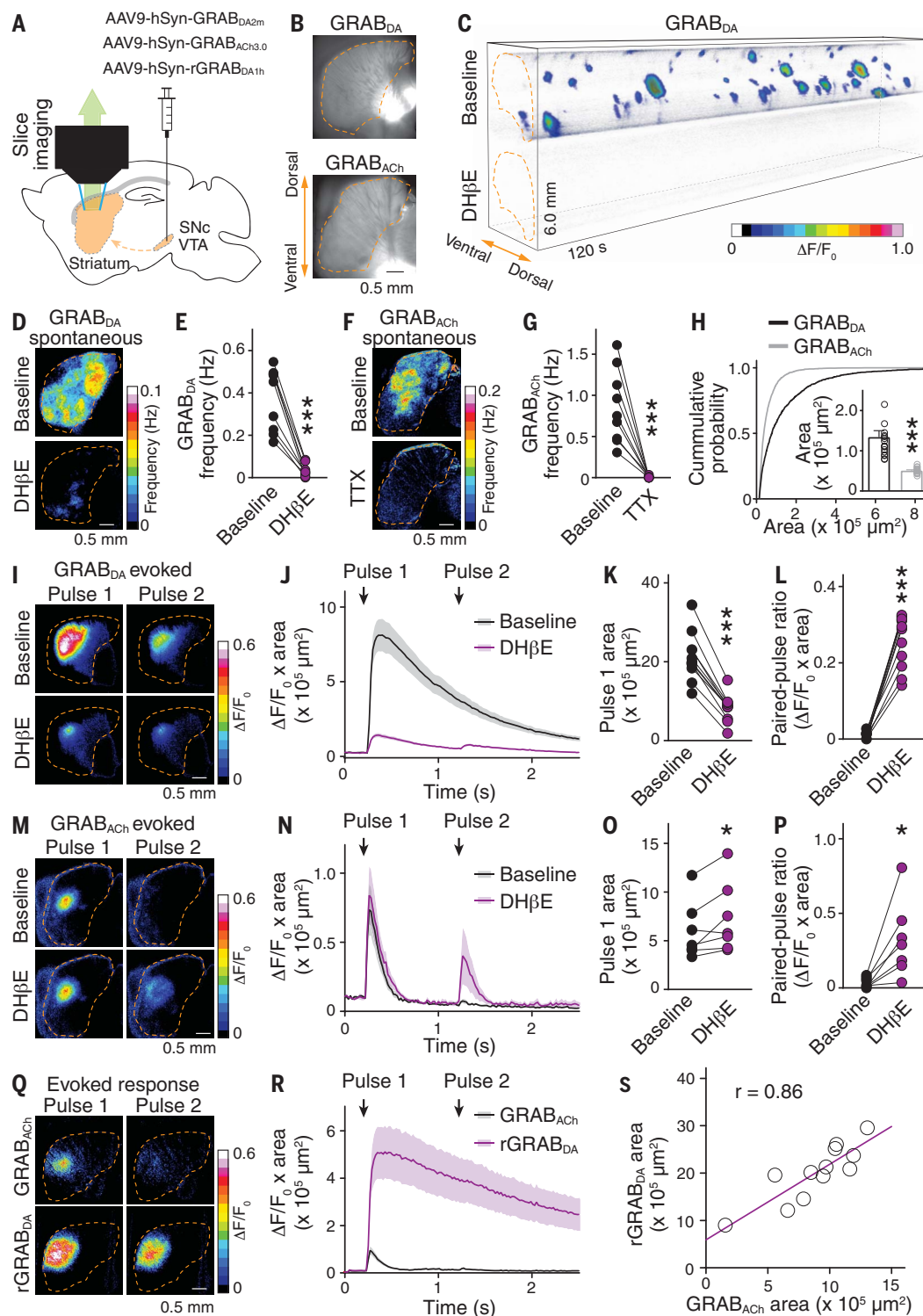
(B) GRAB_{DA} and GRAB_{ACh} expression in striatal slices. Dashed lines (orange) outline the striatum.

(C) Volume-rendered time series of spontaneous GRAB_{DA} fluctuations (expressed as $\Delta F/F_0$, color-coded for magnitude) before (top) and after (bottom) application of DH β E (1 μ M). Areas with $\Delta F/F_0 < 0.02$ were made transparent for clarity.

(D) Example frequency maps and (E) quantification of spontaneous GRAB_{DA} events detected before and after 1 μ M DH β E; $n = 9$ slices from four mice. (F and G) As in (D) and (E) but for GRAB_{ACh} before and after 1 μ M TTX; $n = 9$ slices from three mice.

(H) Comparison of the area covered by GRAB_{DA} and GRAB_{ACh} events; $n = 1010$ events from 17 slices from four mice for GRAB_{DA}, $n = 2087$ events from 14 slices from four mice for GRAB_{ACh}. (I) Example images and (J to L) quantification of GRAB_{DA} fluorescence evoked by paired electrical stimuli (1-s interval) before and after 1 μ M Dh β E; $n = 11$ slices from four mice. (M to P) As I to L, but for GRAB_{ACh}; $n = 7$ slices from three mice. (Q and R) As in (I) and (J) but for simultaneous assessment of GRAB_{ACh} and rGRAB_{DA}; $n = 12$ slices from four mice.

(S) Correlation of areas in (R). Data are mean \pm SEM; * $P < 0.05$, *** $P < 0.001$; Wilcoxon signed-rank tests for (E), (G), (K), (L), (O), and (P); Mann-Whitney rank-sum test for (H).

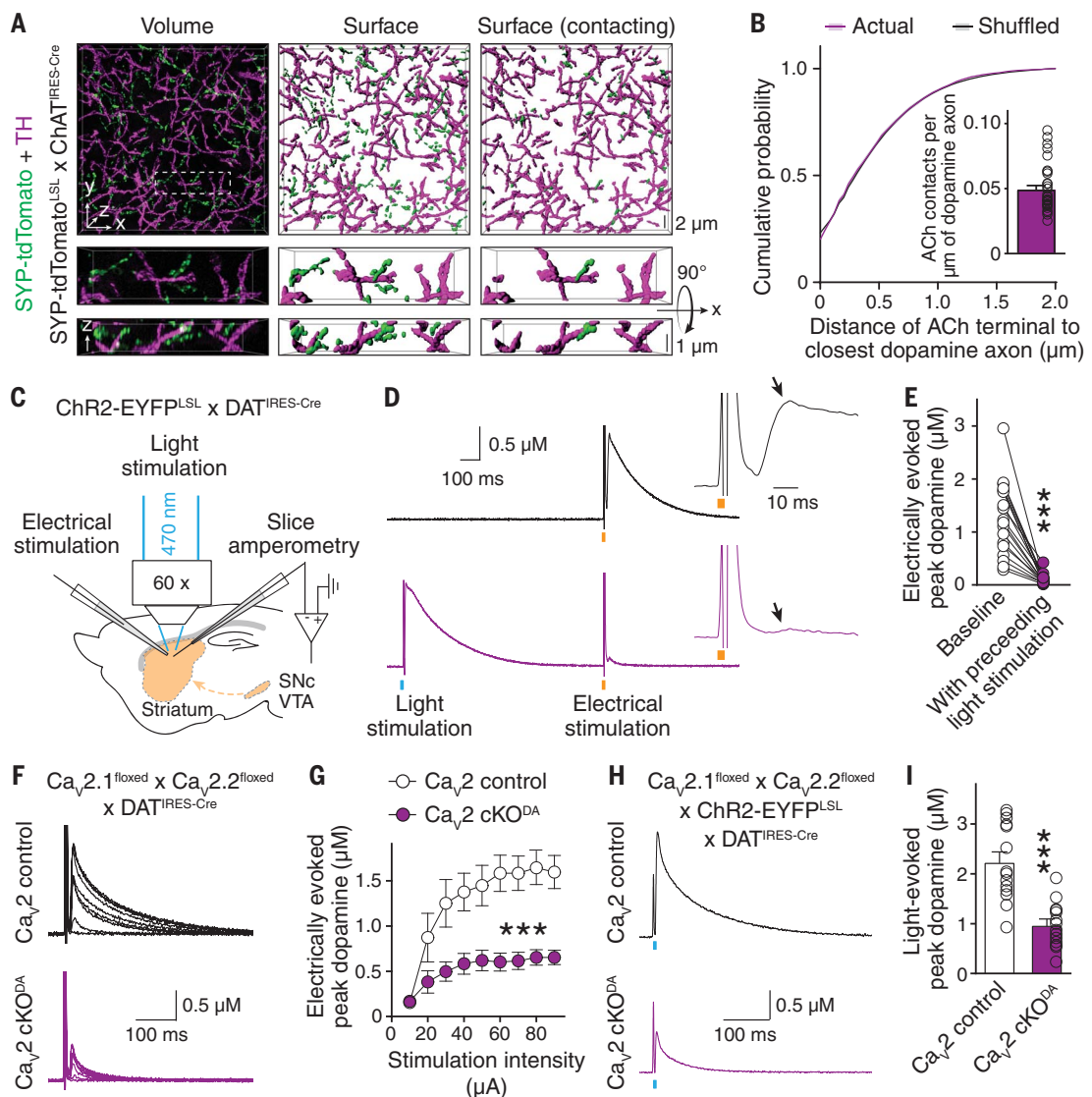


of the vesicles are releasable, and only a subset of the varicosities contains active release sites to respond to action potentials (3, 14, 22). Thus, one way for ACh neurons to boost dopamine release could be by recruiting additional vesicles and/or release sites. To test this possibility, we performed cross-depletion ex-

periments. We expressed the light-activated cation channel channelrhodopsin-2 (ChR2) in dopamine axons and evoked dopamine release with light (to specifically activate dopamine axons) followed by electrical stimulation (to activate dopamine axons and ACh neurons) (Fig. 2C). Electrical stimula-

tion induces dopamine release with two phases (fig. S5), and the second phase is entirely mediated by ACh (12, 14). Preceding light stimulation nearly abolished the second phase (Fig. 2, D and E), indicating that vesicles and release sites are shared between the two release modes.

Fig. 2. ACh triggers dopamine secretion through the same release mechanisms as dopamine neuron action potentials. (A) Example 3D-SIM images of dorsal striatal slices showing dopamine axons (labeled with TH antibodies) and ACh nerve terminals [labeled by crossing Cre-dependent Synaptophysin-tdTomato mice (SYP-tdTomato^{LSL}) with ChAT^{ires-Cre} mice]. Images were obtained by means of (left) volume rendering of an image stack, (middle) surface rendering of detected objects, and (right) surface rendering of ACh terminals that contact dopamine axons (>0 voxel overlap). (B) Comparison of the minimal distance of ACh terminals from the nearest dopamine axons. Controls were generated by averaging 1000 rounds of local shuffling and distance calculation of each ACh terminal within 5 by 5 by 1 μm^3 ; $n = 5482$ objects from 33 images from four mice. (C) Schematic of slice recordings. Chr2-EYFP was expressed in dopamine neurons (by crossing Chr2-EYFP^{LSL} with DAT^{ires-Cre} mice), and dopamine release was measured by using amperometry in dorsal striatal slices in the area of light stimulation. (D) Example traces and (E) quantification of peak amplitude of the second dopamine release phase (arrows) evoked by means of electrical stimulation (orange bar) with (bottom) or without (top) a preceding 1-ms light stimulus (blue bar; 1 s before); $n = 18$ slices from three mice. (F) Example traces and (G) quantification of peak dopamine amplitude (second phase) evoked by means of electrical stimulation in Ca_v2 cKO^{DA} mice (Ca_v2.1 + 2.2 double floxed mice crossed to DAT^{ires-Cre} mice)



and dopamine release was measured by using amperometry in dorsal striatal slices in the area of light stimulation. (D) Example traces and (E) quantification of peak amplitude of the second dopamine release phase (arrows) evoked by means of electrical stimulation (orange bar) with (bottom) or without (top) a preceding 1-ms light stimulus (blue bar; 1 s before); $n = 18$ slices from three mice. (F) Example traces and (G) quantification of peak dopamine amplitude (second phase) evoked by means of electrical stimulation in Ca_v2 cKO^{DA} mice (Ca_v2.1 + 2.2 double floxed mice crossed to DAT^{ires-Cre} mice)

and sibling Ca_v2 control mice; $n = 13$ slices from four mice each [$P < 0.001$ for genotype, stimulation intensity and interaction; two-way analysis of variance (ANOVA); genotype effect reported in the figure]. (H and I) Similar to (F) and (G) but with dopamine release evoked by means of light stimulation in mice expressing Chr2-EYFP transgenically in dopamine neurons; $n = 14$ slices from five mice each. Data are mean \pm SEM; *** $P < 0.001$; Kolmogorov-Smirnov test for (B); Wilcoxon signed-rank test for (E); and Mann-Whitney rank-sum test for (I).

In principle, ACh may trigger dopamine release in three ways. First, because nAChRs [including the $\alpha 6$ - and $\alpha 4$ -containing nAChRs on dopamine axons (8)] are nonselective cation channels (23), Ca²⁺ entry through them might directly trigger dopamine vesicle fusion. Second, nAChR activation might depolarize the dopamine axon membrane and activate low-voltage-gated Ca²⁺ channels to induce dopamine release. Last, nAChR activation on dopamine axons might initiate ectopic action potentials followed by opening of low- and high-voltage-gated Ca²⁺ channels and release.

We started distinguishing between these possibilities by characterizing the Ca²⁺ sources for ACh-induced dopamine release. Double removal of Ca_v2.1 (P/Q-type) and Ca_v2.2 (N-type) channels in dopamine neurons similarly reduced ACh-induced release (the second phase in response to electrical stimulation) and action potential-induced release (by optogenetic activation of dopamine axons) (Fig. 2, F to I, and fig. S5A). Removing Ca_v2.3 (R-type) channels had no effect (fig. S5, B to D). Hence, both release modes rely on these voltage-gated Ca²⁺ channels to a similar extent, ruling out

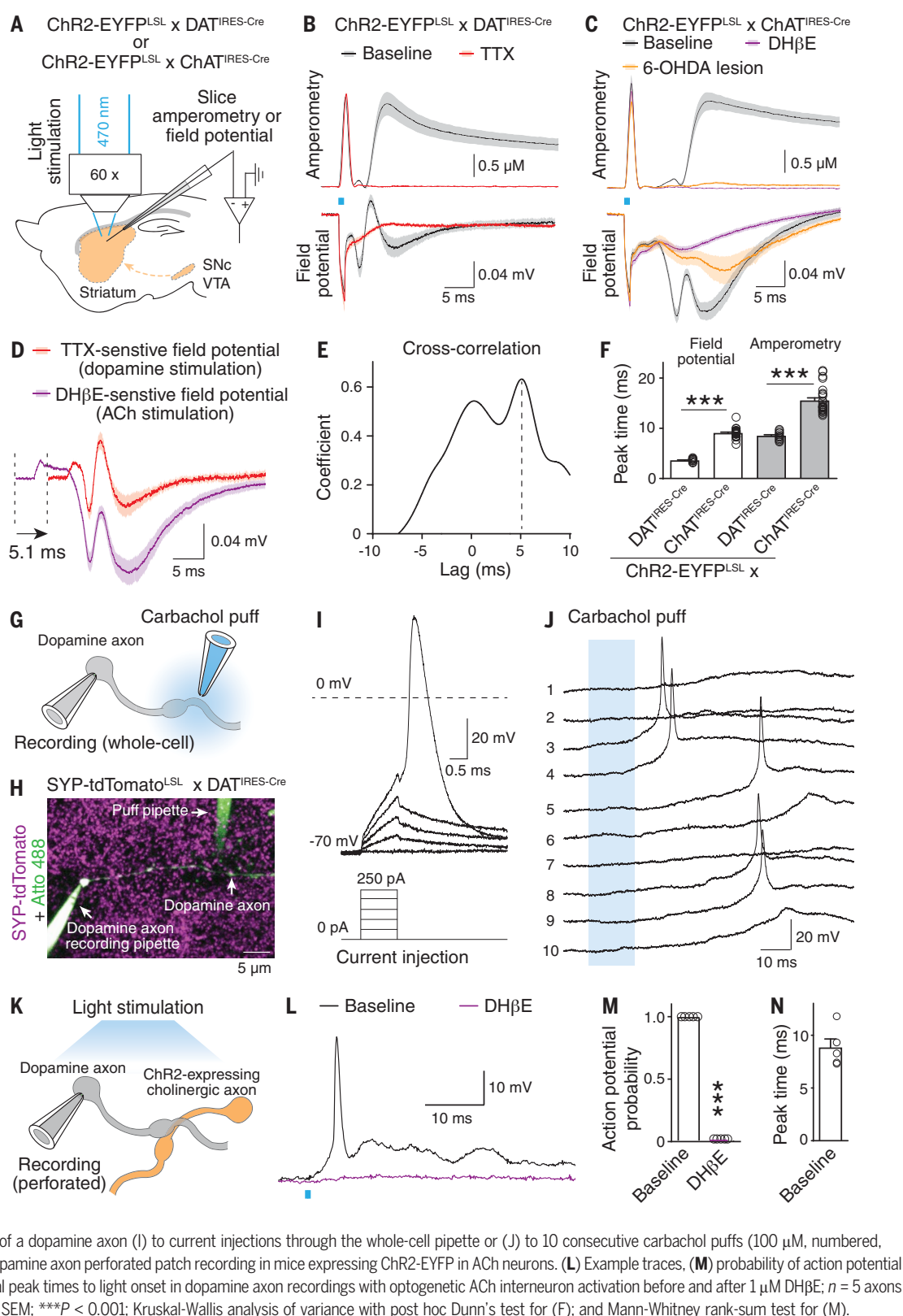
that nAChRs are the main source of Ca²⁺ influx. Because Ca_v2.1 and Ca_v2.2 are high-voltage activated and open efficiently at membrane potentials higher than typical action potential thresholds (24, 25), generating ectopic action potentials in dopamine axons is most likely necessary for ACh to induce dopamine release.

Striatal cholinergic activation induces action potential firing in distal dopamine axons

To test whether ACh can induce dopamine axon firing, we expressed Chr2 in dopamine

Fig. 3. Activation of nAChRs triggers action potentials in striatal dopamine axons.

(A) Schematic of recordings with carbon fiber electrodes in voltage-clamp (0.6 V, amperometric recordings) or current-clamp (no current injection, field potential recordings). (B and C) Average traces of (top) light-evoked dopamine release (amperometry) and (bottom) field potentials in brain slices of mice with ChR2-EYFP in (B) dopamine axons or (C) ACh neurons. Example traces are provided in fig. S7, B and C. Recordings were in ACSF (baseline), (B) in 1 μ M TTX, or (C) in 1 μ M DH β E or (C) after 6-OHDA injection. (B) $n = 12$ slices from three mice each; (C), $n = 25$ slices from six mice (each) for baseline, $n = 21$ slices from six mice (amperometry) and $n = 9$ slices from four mice (field potentials) for DH β E, and $n = 11$ slices from six mice each for 6-OHDA. (D) Comparison of TTX-sensitive and DH β E-sensitive field potentials (obtained through subtraction) (fig. S7, B and C). TTX-sensitive components are right-shifted by 5.1 ms [lag detected in (E)]; n is as in (B) and (C). (E) Cross-correlation of TTX- and DH β E-sensitive components shown in (D). (F) Lag of peak response from the start of the light stimulus; n is as in (B) and (C). (G) Schematic and (H) example two-photon image of direct recording from dopamine axons. Synaptophysin-tdTomato was expressed by using mouse genetics in dopamine axons, the recorded axon was filled with Atto 488 (green) through the recording pipette, and the puff pipette contained carbachol and Atto 488. (I and J) Example responses of a dopamine axon (I) to current injections through the whole-cell pipette or (J) to 10 consecutive carbachol puffs (100 μ M, numbered, 10-s intervals). (K) Schematic of dopamine axon perforated patch recording in mice expressing ChR2-EYFP in ACh neurons. (L) Example traces, (M) probability of action potential firing, and (N) lag of action potential peak times to light onset in dopamine axon recordings with optogenetic ACh interneuron activation before and after 1 μ M DH β E; $n = 5$ axons from three mice. Data are mean \pm SEM; *** $P < 0.001$; Kruskal-Wallis analysis of variance with post hoc Dunn's test for (F); and Mann-Whitney rank-sum test for (M).



or ACh neurons and recorded evoked dopamine release and field potentials in striatal slices using a carbon fiber electrode (Fig. 3A and fig. S6, A and B). Optogenetic activation

of dopamine axons evoked robust dopamine release and a triphasic field potential that was abolished by TTX but insensitive to a range of neurotransmitter receptor blockers

(Fig. 3B and fig. S7A). This indicates that the field potential represents dopamine axon population firing. Optogenetic activation of the cholinergic system produced a similar triphasic

response that was disrupted by DH β E or by 6-hydroxydopamine (6-OHDA) lesion of dopamine axons (Fig. 3C and fig. S6C), demonstrating that it is evoked by nAChR activation and originates from dopamine axons.

The shape of the DH β E-sensitive component of cholinergic activation was similar to the TTX-sensitive component of dopamine axon stimulation (Fig. 3, D and E, and fig. S7, B and C), suggesting that ACh induces firing in dopamine axons. The potential induced through cholinergic activation lagged 5.1 ms behind that of dopamine axon stimulation, which is consistent with the timing of ACh-induced dopamine release (Fig. 3, D to F) (12, 14). Similar to evoked ACh release (fig. S4, E to H), the field potential induced by cholinergic activation exhibited a strong depression during repetitive stimulation that was partially relieved by blocking D2 receptors (fig. S7, D and E).

To investigate the firing of individual axons, we performed direct recordings (26) from genetically labeled dopamine axons (Fig. 3, G and H). Current injection reliably induced large and brief action potentials (amplitude, 113 ± 2 mV; half-width, 0.64 ± 0.03 ms; $n = 24$ axons from nine mice) (Fig. 3I). Upon puffing of carbachol (an nAChR agonist) onto the axon 20 to 40 μ m away from the recording site, 3 out of 14 axons exhibited action potential firing (Fig. 3J and fig. S7F). To test whether action potentials can be induced by endogenous ACh release, we expressed Chr2 in cholinergic interneurons and performed perforated patch recordings from dopamine axons (Fig. 3K). Optogenetic activation of ACh neurons could be tuned to evoke action potentials in all five recorded dopamine axons, and nAChR blockade abolished firing (Fig. 3, L and M). Action potential peak times matched precisely with those of the potentials measured in the field recordings (Fig. 3, F and N).

Striatal ACh and dopamine covary with movement direction

To investigate the functional relevance of ACh-induced dopamine release, we expressed GRAB_{DA} or GRAB_{ACh} together with tdTomato in the right dorsal striatum and monitored the dynamics of the corresponding transmitters by using dual-color fiber photometry in mice exploring an open field arena (Fig. 4A and fig. S8). Because striatal dopamine and ACh might play important roles in movement initiation (27–31), we aligned GRAB_{DA} or GRAB_{ACh} signals to movement onset. We found that both exhibited an increase on average, but there was strong heterogeneity in individual responses (fig. S9).

In previous studies, movement was often restricted to specific directions and/or treated as a scalar quantity (27–31). In our experiments,

mice traveled freely in a large arena and constantly adjusted body posture and movement direction. If only the amplitude of velocity (speed) is considered, spatial information is lost. Hence, we treated velocity as a two-dimensional vector relative to the mouse's head orientation and registered photometry signals to the corresponding velocity plotted in polar coordinates (with angle θ defined as the direction of velocity) (Fig. 4B and fig. S10, A and D). Striatal dopamine and ACh levels were highly correlated with movement direction (Fig. 4, C and E); both exhibited an increase when the animal was turning to the contralateral side or moving forward ($\theta = 0^\circ$ to 120°) and a decrease when the animal was turning to the ipsilateral side or backward ($\theta = 180^\circ$ to 300°). This pattern became more evident when the time series of velocity was right-shifted (fig. S10, B and E), indicating that the velocity peak precedes that of the photometry signal.

When aligned to movement initiations with selected directions, dopamine responses diverged. There was an increase at $\theta = 0^\circ$ to 120° and a decrease at $\theta = 180^\circ$ to 300° , and dopamine transients peaked ~ 150 ms after movement onset (Fig. 4, C and D, and fig. S10, A to C). ACh levels also diverged when aligned to movement onset with selected directions. However, instead of a monotonic decrease, ACh exhibited a decrease followed immediately by an increase for movement initiations with $\theta = 180^\circ$ to 300° (Fig. 4, E and F). This was also detected in the polar coordinates when the velocity time course was right-shifted (fig. S10, D to F).

Striatal ACh contributes to dopamine dynamics

Local inhibition of nAChRs by infusion of DH β E through the optofluid canula slightly decreased dopamine fluctuations (Fig. 4, G and H, and fig. S11, A and B). Dopamine cell bodies and the striatal cholinergic system both drive firing in dopamine axons. The effect of nAChR blockade may be limited because firing of dopamine cell bodies might dominate the signal, and somatic firing could also compensate for the loss of dopamine release induced by blocking nAChRs.

The correlation between dopamine fluctuations and movement direction was largely preserved after unilateral nAChR block with DH β E (Fig. 4I and fig. S11C). However, unilateral DH β E infusion caused a robust reduction in both amplitude and frequency of movement initiations with $\theta = 0^\circ$ to 120° , but only a slight change in amplitude and no change in frequency of those with $\theta = 180^\circ$ to 300° (fig. S11, D to G).

Dopamine neurons respond to salient sensory stimuli (4). We evoked dopamine release by applying 200-ms flashes of light to the open field arena at random intervals (Fig. 4J). Local infusion of DH β E reduced the evoked GRAB_{DA}

response (Fig. 4K). Artificial cerebrospinal fluid (ACSF) infusion also caused a reduction, likely owing to habituation of the mice to the repeated stimuli, that was smaller than the one induced by nAChR blockade (Fig. 4L and fig. S11H). When dopamine and ACh were monitored simultaneously with rGRAB_{DA} and GRAB_{ACh}, respectively, light stimulation evoked a triphasic ACh response, with the initial rise in ACh preceding that of dopamine (Fig. 4M and fig. S11I).

Discussion

Neurotransmitter release from nerve terminals is generally determined by action potentials initiated at the axon initial segment near the soma. Ectopic action potentials are less common, and their functional roles remain elusive (32, 33). Here, we show that ACh induces firing in distal dopamine axons as a physiological mechanism to regulate dopamine signaling. This explains how the striatal cholinergic system broadcasts dopamine release. Ectopic action potentials likely propagate through the axonal network and trigger release along the path. This firing mechanism also accounts for the all-or-none pattern of spontaneous dopamine release and answers why coincident activity in multiple cholinergic neurons is necessary (6): ACh has to quickly depolarize dopamine axons to trigger action potentials before the opening of potassium channels and before ACh is degraded by acetylcholinesterase.

Axonal transmitter secretion is generally viewed to rely on the interplay between firing from the soma (which recruits the entire axon) and local regulation in single nerve terminals (which locally tunes release). We found that local ACh release not only triggers dopamine release (6, 9–12) but hijacks the dopamine axon network to expand signaling with high temporal precision. The exceptionally high levels of nAChRs on dopamine axons (7, 8) might serve to initiate axonal firing. Because presynaptic nAChRs enhance release in multiple types of neurons (34), this axonal firing mechanism might be important beyond the dopamine system.

Individual dopamine terminals are likely indifferent as to where an action potential is generated, and an immediate question is the functional relevance of initiating action potentials in two distinct brain areas. We propose that ACh-induced dopamine axon firing not only represents a distinct input but also sculpts a different dopamine signaling architecture compared with somatic firing. Both phasic somatic and axonal firing induction recruit groups of dopamine axons. Striatal ACh triggers action potentials in neighboring axons centered around the site of ACh release. By contrast, phasic firing in the midbrain recruits cell bodies that share excitatory input, and their axons may or may not be intermingled in the

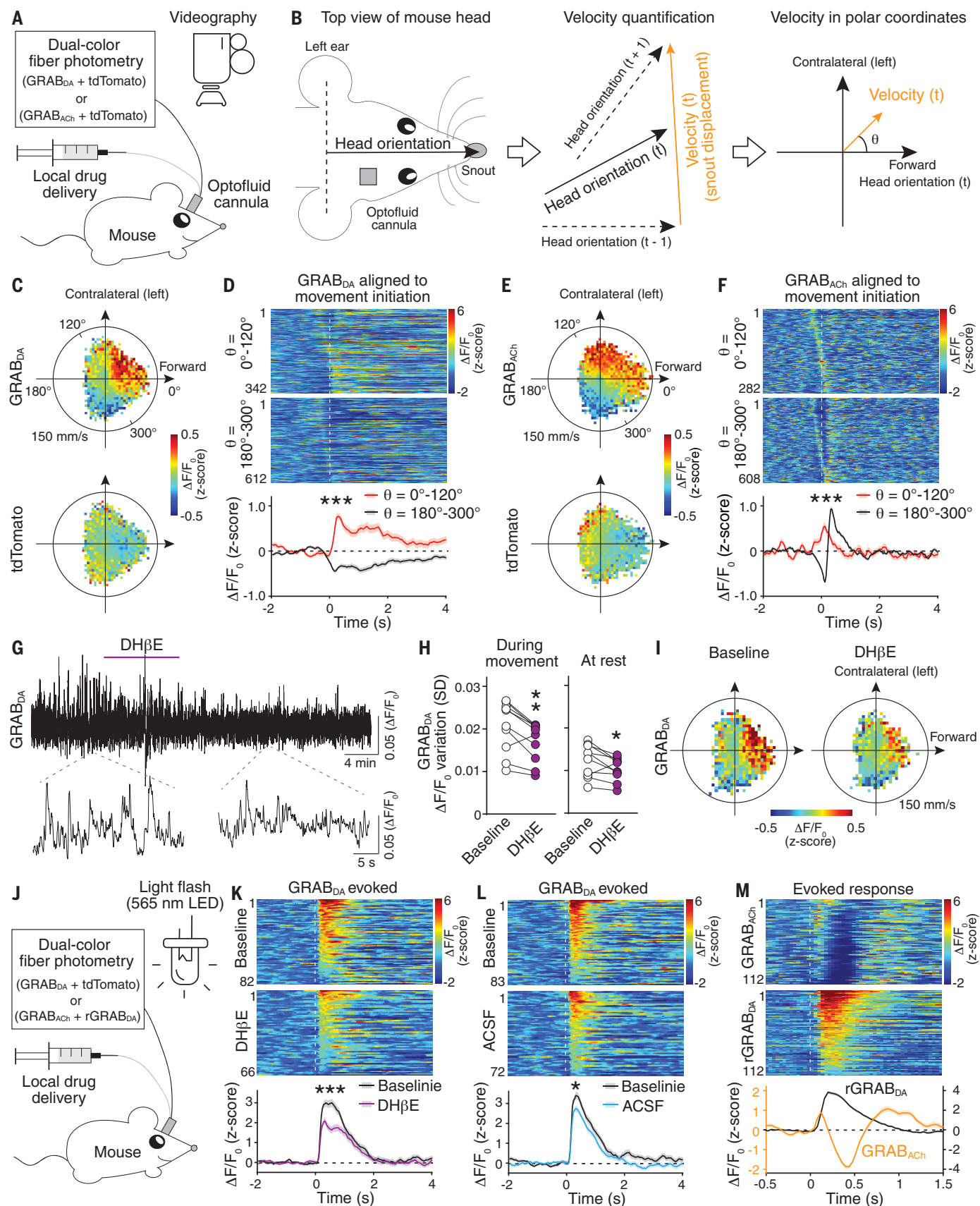


Fig. 4. Dopamine and ACh dynamics correlate with movement direction, and dopamine dynamics are attenuated after blocking nAChRs. (A) Strategy for simultaneous measurements of dopamine or ACh dynamics and behavior in freely moving mice. (B) Fiber photometry and drug delivery were in the right dorsal

striatum by using an optofluid cannula. Head orientation was defined as the direction from the center point between the ears to the snout. Instantaneous velocity at time point t was calculated from the displacement of the snout from $t - 1$ to $t + 1$ and plotted in polar coordinates with head orientation at t defined as $\theta = 0^\circ$. **(C)** Average GRAB_{DA} and tdTomato signals registered to their concurrent velocities in polar coordinates; $n = 10$ mice. **(D)** Individual (heatmap) and average GRAB_{DA} fluctuations aligned to movement initiation (dashed line) with (top) $\theta = 0^\circ$ to 120° or (bottom) 180° to 300° . Heatmaps were sorted by peak time; $n = 342$ events from 10 mice for $\theta = 0^\circ$ to 120° , $n = 612$ events from 10 mice for $\theta = 180^\circ$ to 300° . **(E and F)** As in (C) and (D) but for GRAB_{ACh}; $n = 282$ events from 11 mice for $\theta = 0^\circ$ to 120° , $n = 608$ events from 11 mice for $\theta = 180^\circ$ to 300° . **(G)** Example trace and **(H)** quantification (standard deviation of $\Delta F/F_0$) of

GRAB_{DA} fluorescence before and after DH β E (50 μ M, 1 μ l) delivered through the optofluid canula; $n = 10$ mice. **(I)** Average GRAB_{DA} signals registered to concurrent velocities before and after DH β E; $n = 10$ mice. **(J)** Schematic for measurements of dopamine release induced by 200-ms light flashes in freely moving mice. **(K and L)** Individual (heatmap) and average GRAB_{DA} fluctuations aligned to the light flash (dashed line) before and after local infusion of (K) DH β E or (L) ACSF. (K), $n = 82$ responses from 10 mice for baseline, $n = 66$ responses from 10 mice for DH β E; (L) $n = 83$ responses from 10 mice for baseline, $n = 72$ responses from 10 mice for ACSF. **(M)** Similar to (K) but for simultaneous assessment of GRAB_{ACh} and rGRAB_{DA}; $n = 112$ responses from four mice. Data are mean \pm SEM; *** $P < 0.001$, ** $P < 0.01$, * $P < 0.05$; Mann-Whitney rank-sum tests for areas under the curve (0 to 400 ms) in (D), (F), (K), and (L). Wilcoxon signed-rank test for (H).

striatum (1, 35, 36). Hence, ACh-induced dopamine release might endow dopamine signaling with spatial control over striatal circuitry that is distinct from release induced by activating midbrain somata. Our work further suggests that information flow in dopamine neurons between the midbrain and striatum might be bidirectional. Axon→soma signaling could occur through action potential backpropagation (37, 38) upon striatal cholinergic activity to regulate somatodendritic dopamine release, dendritic excitability, or other midbrain processes.

Roles for striatal dopamine and ACh are under intense investigation, and both excitation and inhibition in the firing have been associated with spontaneous movement (27, 28, 30, 31). We demonstrate that striatal dopamine and ACh not only correlate with movement initiation but also with its direction, potentially explaining the heterogeneity of their responses at movement onset. The findings that ACh and dopamine covary with movement direction and that ACh enhances dopamine dynamics suggest that the two systems are coordinated for their roles in motor control (27). These findings fit well with classical observations that unilateral lesions of dopamine or ACh systems induce asymmetric behavior and support that dynamic transmitter balance between hemispheres is important for adjusting body posture (29, 39). Last, we observed that dopamine dynamics are regulated by nAChRs regardless of movement state, which indicates that ACh-induced dopamine release likely has additional physiological roles.

REFERENCES AND NOTES

- W. Matsuda et al., *J. Neurosci.* **29**, 444–453 (2009).
- J. D. Berke, *Nat. Neurosci.* **21**, 787–793 (2018).

- C. Liu, P. Goel, P. S. Kaeser, *Nat. Rev. Neurosci.* **22**, 345–358 (2021).
- E. S. Bromberg-Martin, M. Matsumoto, O. Hikosaka, *Neuron* **68**, 815–834 (2010).
- C. J. Wilson, *Neuron* **45**, 575–585 (2005).
- S. Threlfell et al., *Neuron* **75**, 58–64 (2012).
- N. Le Novère, M. Zoli, J.-P. Changeux, *Eur. J. Neurosci.* **8**, 2428–2439 (1996).
- I. W. Jones, J. P. Bolam, S. Wonnacott, *J. Comp. Neurol.* **439**, 235–247 (2001).
- M. F. Giurgeff, M. L. Le Floch, J. Glowinski, M. J. Besson, *J. Pharmacol. Exp. Ther.* **200**, 535–544 (1977).
- F.-M. Zhou, Y. Liang, J. A. Dani, *Nat. Neurosci.* **4**, 1224–1229 (2001).
- R. Cachope et al., *Cell Rep.* **2**, 33–41 (2012).
- L. Wang et al., *J. Physiol.* **592**, 3559–3576 (2014).
- F. Sun et al., *Nat. Methods* **17**, 1156–1166 (2020).
- C. Liu, L. Kershuberg, J. Wang, S. Schneberger, P. S. Kaeser, *Cell* **172**, 706–718.e15 (2018).
- M. Jing et al., *Nat. Methods* **17**, 1139–1146 (2020).
- A. A. Mamaligas, C. P. Ford, *Neuron* **91**, 574–586 (2016).
- J. M. Schulz, M. J. Oswald, J. N. J. Reynolds, *J. Neurosci.* **31**, 11133–11143 (2011).
- G. Morris, D. Arkadir, A. Nevet, E. Vaadia, H. Bergman, *Neuron* **43**, 133–143 (2004).
- Y. Cai, C. P. Ford, *Cell Rep.* **25**, 3148–3157.e3 (2018).
- C. Straub, N. X. Tritsch, N. A. Hagan, C. Gu, B. L. Sabatini, *J. Neurosci.* **34**, 8557–8569 (2014).
- H. T. Chang, *Brain Res. Bull.* **21**, 295–304 (1988).
- D. B. Pereira et al., *Nat. Neurosci.* **19**, 578–586 (2016).
- E. R. Decker, J. A. Dani, *J. Neurosci.* **10**, 3413–3420 (1990).
- R. G. Held et al., *Neuron* **107**, 667–683.e9 (2020).
- J. Yang et al., *Front. Cell. Neurosci.* **13**, 317 (2019).
- A. Ritzau-Jost et al., *Cell Rep.* **34**, 108612 (2021).
- M. Howe et al., *eLife* **8**, e44903 (2019).
- P. D. Dodson et al., *Proc. Natl. Acad. Sci. U.S.A.* **113**, E2180–E2188 (2016).
- S. Kaneko et al., *Science* **289**, 633–637 (2000).
- M. W. Howe, D. A. Dombeck, *Nature* **535**, 505–510 (2016).
- J. A. da Silva, F. Tecuapetla, V. Paixão, R. M. Costa, *Nature* **554**, 244–248 (2018).
- T. Dugladze, D. Schmitz, M. A. Whittington, I. Vida, T. Gloveli, *Science* **336**, 1458–1461 (2012).
- M. E. J. Sheffield, T. K. Best, B. D. Mensh, W. L. Kath, N. Spruston, *Nat. Neurosci.* **14**, 200–207 (2011).
- J. A. Dani, D. Bertrand, *Annu. Rev. Pharmacol. Toxicol.* **47**, 699–729 (2007).
- N. Eshel, J. Tian, M. Bukwich, N. Uchida, *Nat. Neurosci.* **19**, 479–486 (2016).
- J. G. Parker et al., *Proc. Natl. Acad. Sci. U.S.A.* **107**, 13491–13496 (2010).

- A. A. Grace, B. S. Bunney, *Science* **210**, 654–656 (1980).
- L. J. Gentet, S. R. Williams, *J. Neurosci.* **27**, 1892–1901 (2007).
- N. F. Parker et al., *Nat. Neurosci.* **19**, 845–854 (2016).
- C. Liu, Data table for an action potential initiation mechanism in distal axons for the control of dopamine release. Zenodo (2022); doi: 10.5281/zenodo.6342359.
- C. Liu, Matlab script for object recognition and analysis. Zenodo (2022); doi: 10.5281/zenodo.6342367.

ACKNOWLEDGMENTS

We thank C. Qiao, M. Han, and J. Wang for technical assistance; N. Uchida, M. Watabe-Uchida, and I. Tsutsui-Kimura for advice on setting up fiber photometry; A. van den Maagdenberg for Ca_v2.1^{flxed} mice and T. Schneider for Ca_v2.3^{flxed} mice; and C. Harvey, B. Sabatini, W. Regehr, N. Uchida, J. Williams, and R. Wise for discussions and comments on the manuscript. We acknowledge the Neurobiology Imaging Facility (supported by P3ONS072030) and Cell Biology Microscopy Facility for microscope availability and advice. **Funding:** This work was supported by the NIH (R01NS103484 and R01NS083898 to P.S.K. and NINDS Intramural Research Program Grant NS003135 to Z.M.K.), the European Research Council (ERC CoG 865634 to S.H.), the German Research Foundation (DFG; HA6386/10-1 to S.H.), the Dean's Initiative Award for Innovation (to P.S.K.), a Harvard-MIT Joint Research Grant (to P.S.K.), and a Gordon family fellowship (to C.L.). X.C. is a visiting graduate student and received a PhD Mobility National Grants fellowship from Xi'an Jiaotong University/China Scholarship Council. **Author contributions:** Conceptualization: C.L. and P.S.K. Methodology: C.L., X.C., A.R.-J., P.F.K., Z.M.K., S.H., and P.S.K. Investigation: C.L., X.C., A.R.-J., and P.F.K. Resources: Y.L. Visualization: C.L., A.R.-J., P.F.K., and P.S.K. Funding acquisition: P.S.K. Project administration: C.L. and P.S.K. Supervision: C.L. and P.S.K. Writing, original draft: C.L. and P.S.K. Writing, review and editing: C.L., X.C., A.R.-J., P.F.K., Y.L., Z.M.K., S.H., and P.S.K. **Competing interests:** Y.L. is listed as an inventor on a patent application (PCT/CN2018/107533) describing GRAB probes. The other authors declare no competing interests. **Data and material availability:** All data and code are available at Zenodo (40, 41).

SUPPLEMENTARY MATERIALS

science.org/doi/10.1126/science.abn0532
Materials and Methods
Figs. S1 to S11
References (42–48)
MDAR Reproducibility Checklist
Movies S1 to S2

31 October 2021; accepted 23 February 2022
10.1126/science.abn0532